S. F. and Y. G. appreciated the support of the Deutscher Akademischer Austauschdienst e.V. and the Foreign Relations unit of the Technische Universität Berlin, respectively.

References

[1]Bradshaw, P., "Turbulent Secondary Flow," *Annual Review of Fluid Mechanics*, Vol. 19, 1987, pp. 53–74.

[2]Demuren, A. O., and Rodi, W., "Calculations of Turbulence-Driven Secondary Motion in Non-Circular Ducts," *Journal of Fluid Mechanics*, Vol. 140, 1984, pp. 189–222.

[3]Launder, B. E., and Rodi, W., "The Turbulent Wall Jet," *Annual Review of Fluid Mechanics*, Vol. 15, 1983, pp. 429–459.

[4]Rodi, W., "A New Algebraic Relation for Calculating the Reynolds Stresses," ZAMM, Vol. 56, No. 3, 1976, pp. T219–T221.

[5]Gatski, T. B., and Speziale, C. G., "On Explicit Algebraic Stress Models for Complex Turbulent Flows," *Journal of Fluid Mechanics*, Vol. 254, 1993, pp. 59–75.

[6]Rivlin, R. S., and Ericksen, J. L., "Stress-Deformation Relations for Isotropic Materials," *Journal of Rational Mechanics and Analysis*, Vol. 4, 1955, pp. 323–425.

[7]Speziale, C. G., Sarkar, S., and Gatski, T. B., "Modelling the Pressure-Strain Correlation of Turbulence: An Invariant Dynamical Systems Approach," *Journal of Fluid Mechanics*, Vol. 227, 1991, pp. 245–272.

[8]Gibson, M. M., and Launder, B. E., "Ground Effects on the Pressure Fluctuations in the Atmospheric Boundary Layer," *Journal of Fluid Mechanics*, Vol. 86, 1978, pp. 491–511.

[9]Rung, T., Thiele, F., and Fu, S., "On the Realizability of Nonlinear Stress-Strain Relationships for Reynolds Stress Closures," *Flow, Turbulence, and Combustion*, Vol. 60, No. 4, 1999, pp. 333–359.

[10]Demuren, A. O., "On the Generation of Secondary Motion in Circular-to-Rectangular Transition Ducts," AIAA Paper 93-0681, 1993.

[11]Sotiropoulos, F., and Patel, V. C., "Prediction of Turbulent Flow Through a Transition Duct Using a Second-Moment Closure," *AIAA Journal*, Vol. 27, No. 11, 1994, pp. 2194–2204.

R. M. C. So
Associate Editor

Pressure-Sensitive Paint Measurements in Planar Transonic Nozzle Flow

Johan Gullman-Strand*
Royal Institute of Technology, S-100 44 Stockholm, Sweden
and
Bruce F. Carroll†
University of Florida, Gainesville, Florida 32611-6250

Introduction

DUTTON and Addy performed series expansion solutions for the transonic flowfield in the throat region of axisymmetric[1] and annular[2] nozzles. Their results compared well with experimental data. The solution method utilized an expansion parameter defined so as to improve the solution convergence even for small wall radii of curvature. For the annular case, the perturbation velocity components were expanded in power series in the parameter ε, defined as $\varepsilon = 1/(\bar{R}_c + \eta)$, where $\bar{R}_c = R_c/D$ is the average dimensionless wall radius of curvature at the throat, D is the throat half height, and η is an arbitrary parameter included to improve the solution convergence. Order of magnitude assumptions required in the solution method limited the analysis of Ref. 2 to small flow inclination angles. To overcome this limitation, Carroll and Dutton[3] performed the series expansion solution for the case of annular throat flow inclined at arbitrary but large angles to the nozzle axis of symmetry, that is, for radial or nearly radial supersonic nozzles. The solution is also applicable to the two-dimensional planar case. Although this solution was shown to satisfy several internal checks for consistency, it was never verified experimentally. The purpose of this Note is to perform an experimental verification of the transonic solution for the planar case of Ref. 3. Pressure-sensitive paint (PSP) was selected as the primary measurement tool because of its high spatial resolution in regions of strong gradients. Thus, a secondary purpose of this paper is to evaluate the PSP technique for this type of flow.

Formulation and Experimental Setup

The nozzle geometry for the planar case is shown in Fig. 1. The origin of the x–y coordinate system is located at the minimum area location and equidistant between the nozzle walls. The x axis points in the mean flow direction, and the orthogonal y axis maintains a right-handed system. The walls are symmetric about the x axis. The governing equations are the irrotationality condition and the gasdynamic equation. The boundary conditions are that the nozzle walls are streamlines. A regular perturbation solution about a uniform sonic flow is then obtained with the details given by Carroll and Dutton.[3]

The PSP was a dual-probe pressure/temperature sensitive coating with characteristics similar to that reported by Carroll et al.[4] The side wall of the test section was made from aluminum, which serves as a thermal sink and tends to mask the expected wall temperature variations. Because of this, the test region did not exhibit significant spatial variations in temperature; thus, only the pressure sensing function of the dual-probe PSP was utilized. The PSP data collection and analysis methods were similar to those reported by Morris et al.[5] Intensity data were converted to pressure with a fourth-order polynomial calibration function:

$$\frac{P}{P_{\text{ref}}} = \sum_{i=0}^{n} c_i \left(\frac{I_{\text{ref}}}{I}\right)^i, \qquad n = 4 \tag{1}$$

The constants $c_0, \ldots, c_4$ were determined by curvefitting calibration data in the range from 13.8 to 179.3 kPa. Pressure data were converted to Mach number using standard isentropic relations.

To smooth out any peaks resulting from the misalignment of the wind-on and reference images and imperfections in the paint, a filter of both averaging and median was applied. The averaging was done over a local 5×5 pixel matrix and the median filter used the median of the element values of the same matrix:

$$M = \alpha\bar{M} + (1 - \alpha)\tilde{M}, \qquad \alpha = 0.25 \tag{2}$$

with $\bar{M}$ as the average and $\tilde{M}$ as the median. By the use of the median filtering, the sharp edges occurring at the walls were not smoothed out as would be the case of pure averaging.

The experiments were conducted in a blowdown wind tunnel at the University of Florida. Looking in the flow direction, the right wall was a flat Plexiglas plate, and the left wall was a flat aluminum test plate covered with primer and PSP. Two different aluminum plates were tested. The first had eight pressure taps along the centerline and seven T-type thermocouples. The second test plate had 15 pressure taps, 9 of them in a 3×3 matrix in the throat region and the rest along the centerline. The second plate also had two T-type thermocouples along the centerline. Two symmetric nozzle blocks, with circular arc throat profiles, were mounted in the top and bottom walls

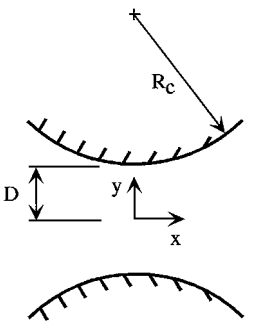

Fig. 1 Definition of coordinate system for symmetric planar nozzle throat.

Received 9 September 1999; revision received 16 May 2000; accepted for publication 25 May 2000.

*Graduate Student, Department of Mechanics.

†Associate Professor, Department of Aerospace Engineering, Mechanics, and Engineering Science, 231 Aerospace Building. Member AIAA.

to form the convergent–divergent nozzle. The throat half-height was $D = 15.0$ mm, and the width was 38.1 mm. The dimensionless wall radii of curvature was equal to $R_c/D = 1.0$ and 2.0.

Two filtered tungsten-halogen lamps [450 nm, 40 nm full width at half maximum (FWHM)] excited the PSP. The PSP had dual properties with emissions in the 550-nm band for temperature and the 650-nm band for pressure. The collection optics included a 40-nm FWHM bandpass filter centered at 650 nm to reject the excitation light and the temperature probe emission. Intensities were then measured with a 14-bit, 512 × 512 pixel cooled charge-coupled device camera. A 50-mm focal length lens yielded an effective pixel density of 36.2 pixels/cm in the image.

When the tests were performed, the tunnel was run until the plate had reached a steady-state temperature distribution. A series of 20 wind-on images were then taken and averaged to reduce shot noise. The mean intensity in the region of interest for a single image was 76,000 electrons, which, when accounting for the 20-image frame averaging, yielded a mean shot noise of 0.08%. A similar procedure was used to collect the wind-off reference intensities. The wind-off reference image was collected at the end of the run to minimize temperature effects. Digitization noise in the mean intensity value was 0.006%. Thus, the total uncertainty in the mean intensity measurement was 0.08% (shot noise limited measurement). This corresponds to a random uncertainty of 0.32% in the pressure ratio, P/P_{ref}.

For calibration purposes, the test section was closed off and served as a calibration chamber. The pressure could be regulated from 13.8 to 179.3 kPa with an accuracy of ±0.14 kPa. This made it possible to perform calibrations with the same light conditions as the wind-on and reference measurements. The combined uncertainty in the pressure from all sources was 0.45% for a typical measurement location.

Results

Because the theory provides solutions in terms of local dimensionless velocities, the pressure data from the PSP were converted to Mach number for comparison purposes. The convergence parameter η was introduced in the expansion parameter ε as $\varepsilon = 1/(R_c/D + \eta)$. When $\varepsilon \to 1$ (i.e., as the wall radius of curvature was decreased below $R_c/D = 1.0$ or 2.0), the convergence of the code improved with increasing η. Based on a convergence study and the results of Carroll and Dutton,[3] a value of $\eta = 2$ was found to be suitable and was used in the rest of this study.

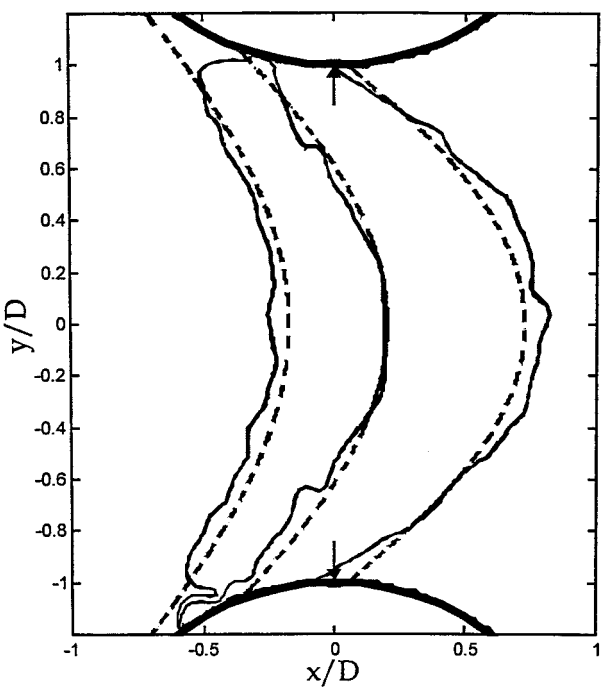

Fig. 2 Mach number contours obtained from PSP (——) and theory (– – –) with the $R_c/D = 1.0$ nozzle blocks; Mach number $M = 0.8$, 1.0, and 1.3.

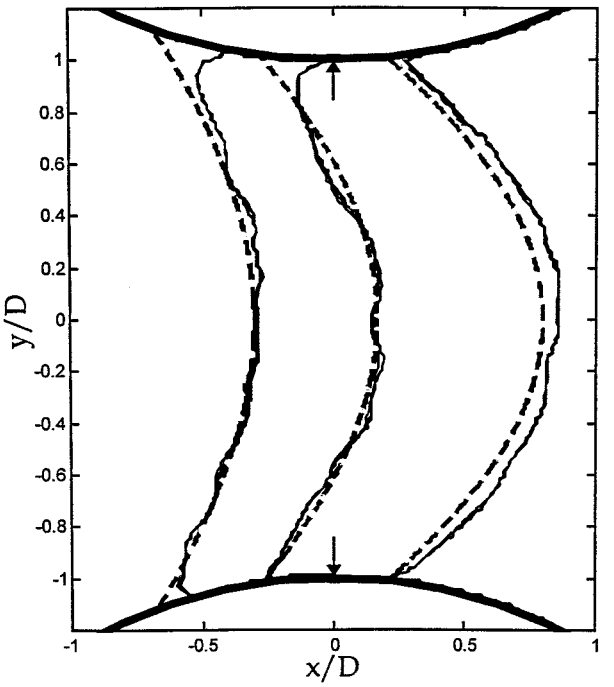

Fig. 3 Mach number contours obtained from PSP (——) and theory (– – –) with the $R_c/D = 2.0$ nozzle blocks; Mach number $M = 0.8$, 1.0, and 1.3.

A comparison between theory and measurements is visualized in the contour plots of Figs. 2 and 3 with $R_c/D = 1.0$ and 2.0, respectively. The nozzle walls are indicated as dark lines at the top and bottom of the symmetric geometry. The small arrows at $x = 0$ denote the throat location. Near the centerline, the Mach number distributions were accurately predicted, but the comparison of the whole flowfield showed discrepancies near the nozzle walls. A possible source for the erroneous behavior close to the wall was reflections in sharp corners. Because the nozzle had a width of 38.1 mm, the exposing light was partly reflected on the top and bottom nozzle walls as well as off the PSP-coated side plate. The problem can be reduced by using diffuse reflection according to Davies et al.,[6] but the disturbance did not affect the general data. Overall, the theory (dashed lines) tended to overpredict the subsonic flow and underpredict the supersonic flow. The difference in Mach number between theory and experiment was less then 0.035 for the range from 0.8 to 1.3 for both R_c/D. The optical configuration made it possible to resolve the pressure data in steps of 3.63 kPa/pixel, corresponding to Mach number gradient of 0.032/pixel. Thus, the difference between theory and measurements is on the order of the discretization level of the PSP measurement. This demonstrates the ability to perform high-resolution pressure measurements in accelerating flows of this type.

Conclusions

A comparison was made between experiments and theory for the flow in the transonic region of a supersonic planar nozzle. The main experimental technique was PSP, and the theory was based on a transonic perturbation solution. Agreement between theory and experiment appears to be better for the subsonic and sonic portions of the flow. However, agreement at all Mach numbers considered (0.8–1.3) was within the experimental uncertainty, indicating the validity of the transonic solution of Carroll and Dutton.[3]

Acknowledgments

We wish to thank Arne Johansson for his support of Johan Gullman-Strand during this work. We also thank Paul Hubner and Andy Winslow for assistance with the experiments.

References

[1] Dutton, J. C., and Addy, A. L., "Transonic Flow in the Throat Region of Axisymmetric Nozzles," *AIAA Journal*, Vol. 19, No. 6, 1981, pp. 801–804.

[2]Dutton, J. C., and Addy, A. L., "Transonic Flow in the Throat Region of Annular Supersonic Nozzles," *AIAA Journal*, Vol. 19, No. 9, 1982, pp. 1236–1243.

[3]Carroll, B. F., and Dutton, J. C., "Transonic Flow in the Throat Region of Radial or Nearly Radial Supersonic Nozzles," *AIAA Journal*, Vol. 23, No. 7, 1985, pp. 1127–1129.

[4]Carroll, B. F., Hubner, J. P., Schanze, K. S., Bedlek, J., and Morris, M. J., "Pressure and Temperature Measurements with a Dual-Luminophore Coating," *Proceedings of the ICIASF99 Record*, Inst. of Electrical and Electronics Engineers, New York, 1999, pp. 18.1–18.8.

[5]Morris, M. J., Donovan, J., Kegelman, J., Schwab, S., and Levy, R., "Aerodynamic Applications of Pressure Sensitive Paint," *AIAA Journal*, Vol. 31, No. 3, 1993, pp. 419–425.

[6]Davies, A., Bedwell, D., Dunleavy, M., and Brownjohn, N., "Pressure Sensitive Paint Limitations and Solutions," *Proceedings of the 7th International Symposium on Flow Visualization*, 1995, pp. 11–21.

R. P. Lucht
Associate Editor

Effects of Vibrational Relaxation on Bow Shock Standoff Distance for Nonequilibrium Flows

A. F. P. Houwing,* S. Nonaka,† H. Mizuno,†
and K. Takayama‡
Tohoku University, Sendai 980-8577, Japan

I. Introduction

PREVIOUS work by Hornung[1] considered the dependence of the normalized shock standoff distance on the normalized dissociation rate immediately after the normal shock in the simple case of a diatomic gas with only one reaction. His work allowed the dissociative nonequilibrium effects on the flowfield to be correlated for this specialized case. More recently, Hornung and Wen[2] extended this previous work to complex gas mixtures with many species and many reactions and to correct the correlation so that the additional parameter of the normalized freestream kinetic energy is accounted for. For the cases that they were considering, dissociative effects dominated the flowfield behavior. However, at somewhat lower specific total enthalpies, vibrational nonequilibrium behavior is dominant and can affect the shock standoff distance in a manner that is analogous to the dissociation cases. Because of this, we have applied their analytic approach to the case where vibrational relaxation effects are important and use the theoretical predictions as a basis for correlating recent ballistic range data. Though the analysis can be extended to account for a nonequilibrium freestream upstream of the bow shock, we limit ourselves to an equilibrium freestream in the current work.

II. Theoretical Considerations

Following Hornung and Wen,[2] we consider the conditions on the stagnation streamline along the symmetry axis between the shock and the stagnation point. The momentum and energy equations for inviscid adiabatic flow along this streamline, in the shock's frame of reference, are given by

$$\mathrm{d}p + \rho u\,\mathrm{d}u = 0 \tag{1}$$

$$\mathrm{d}h + u\,\mathrm{d}u = 0 \tag{2}$$

respectively, where p, ρ, u, and h are the pressure, density, flow speed, and specific enthalpy, respectively. From these two equations, one obtains the following relationship between the changes in the pressure and the specific enthalpy:

$$\mathrm{d}p = \rho\,\mathrm{d}h \tag{3}$$

For the case of a molecular gas, for which the vibrational modes are in equilibrium with each other at a vibrational temperature T_{vib}, while the rotational and translational modes are in equilibrium with each other at a temperature T, the entropy change per unit mass is given by[3]

$$\mathrm{d}s = (1/T)\,\mathrm{d}e + (p/T)\,\mathrm{d}(1/\rho) + [(1/T_{\mathrm{vib}}) - (1/T)]\,\mathrm{d}e_{\mathrm{vib}} \tag{4}$$

where e is the internal energy per unit mass and e_{vib} is the internal energy per unit mass due to vibrational excitation. In the case of a mixture of M atomic and diatomic constituents, N of which are molecular species that have vibrational degrees of freedom, this equation can be generalized to give

$$\mathrm{d}s = \frac{1}{T}\,\mathrm{d}e + \frac{p}{T}\,\mathrm{d}\left(\frac{1}{\rho}\right) + \sum_{i=1}^{i=N} c_i \left(\frac{1}{T_{\mathrm{vib},i}} - \frac{1}{T}\right)\mathrm{d}e_{\mathrm{vib},i} \tag{5}$$

where the subscript i identifies the chemical species; c_i is the mass fraction of species i; $e_{\mathrm{vib},i}$ is the internal energy per unit mass of a molecular species due to its vibrational excitation; the diatomic species are identified by values of i, where $1 \le i \le N$; and atomic species are identified by values of i, where $(N+1) \le i \le M$.

From Eq. (3) and the relationship between the specific internal energy, the specific enthalpy, the pressure, and the density, the only entropy change that occurs along the stagnation streamline is that associated with vibrational excitation. That is,

$$\mathrm{d}s = \sum_{i=1}^{i=N} c_i \left(\frac{1}{T_{\mathrm{vib},i}} - \frac{1}{T}\right)\mathrm{d}e_{\mathrm{vib},i} \tag{6}$$

Considering the internal degrees of freedom, we note that each species will have specific internal energy of translation

$$e_{\mathrm{trans},i} = \tfrac{3}{2} R_i T \tag{7}$$

where R_i is the gas constant for species i. In addition, each of the molecular species will have specific internal energy of rotation

$$e_{\mathrm{rot},i} = R_i T \tag{8}$$

and specific internal energy of vibration

$$e_{\mathrm{vib},i} = \frac{R_i \theta_{\mathrm{vib},i}}{\exp(\theta_{\mathrm{vib},i}/T_{\mathrm{vib},i}) - 1} \tag{9}$$

where $\theta_{\mathrm{vib},i}$ is the characteristic temperature of vibration of diatomic species i. Using the relationship between specific enthalpy, specific internal energy, and pressure, the specific enthalpy is then given by

$$h = \left[\frac{3}{2}\sum_{i=1}^{i=M} c_i R_i + \sum_{i=1}^{i=N} c_i R_i\right] T + \sum_{i=1}^{i=N} c_i e_{\mathrm{vib},i} + \frac{p}{\rho} \tag{10}$$

Defining two mass-averaged gas constants, as follows

$$\bar{R}_{\mathrm{vib}} = \sum_{i=1}^{i=N} c_i R_i \tag{11}$$

$$\bar{R} = \sum_{i=1}^{i=M} c_i R_i \tag{12}$$

and assuming an ideal thermal equation of state, we can rewrite the specific enthalpy as

$$h = \left[\frac{5}{2} + \frac{\bar{R}_{\mathrm{vib}}}{\bar{R}}\right]\frac{p}{\rho} + \sum_{i=1}^{i=N} c_i e_{\mathrm{vib},i} \tag{13}$$

Received 3 May 1999; revision received 6 December 1999; accepted for publication 30 March 2000.

*Visiting Professor, Shock Wave Research Center, Institute of Fluid Science; currently Senior Lecturer, Faculty of Science, Department of Physics, Australian National University, Canberra, Australian Capital Territory 0200, Australia.

†Graduate Student, Shock Wave Research Center, Institute of Fluid Science.

‡Director, Shock Wave Research Center, Institute of Fluid Science.